Journal of Applied Physics

AIP Publishing

Investigating the Ions Emitted by Multiply Charged Ionic Liquids from a Porous Electrospray Ion Source

Szymon Dworski[1, a)] and Charlie N. Ryan[1, b)]
University of Southampton, Southampton, Hampshire, United Kingdom

(Dated: 16 August 2024)

A porous electrospray ion source was tested with three ionic liquids in order to investigate the effects of ionic liquid properties on the sizes of ion clusters emitted by purely ionic electrospray sources. Two of the ionic liquids, bis(1-ethyl-3-methylimidazolium) tetrathiocyanatocobaltate and 1,6-bis(3-methylimidazolium-1-yl)hexane bis(trifluoromethylsulfonyl)amide, were selected due to them having a dication or dianion, which were termed multiply charged ionic liquids due to them containing anions or cations with more than one charge within them. These were selected in order to investigate ionic clustering within electrospray ion emission, and were compared against one of the most common ionic liquids, EMI-BF_4. The current-voltage data showed that EMI-BF_4 emitted similar levels of current to bis(1-ethyl-3-methylimidazolium) tetrathiocyanatocobaltate, even though the latter liquid had significantly lower conductivity and higher viscosity, suggesting an improvement in current speculated to be due to the extra charges contained by the ions. TOF and RPA data are provided, showing all three liquids emitting only ions comprising of monomers, dimers, trimers and quadramers, with some of the 1,6-bis(3-methylimidazolium-1-yl)hexane bis(trifluoromethylsulfonyl)amide data indicating heavier species emission. The data also suggested that the multiply charged ionic liquids produced ions which have two anions or cations attached, termed 'double ions', with these ions have not been previously reported using porous electrospray sources. Furthermore it was found that the dimers emitted by both of the multiply charged ionic liquids seemed to be more stable than EMI-BF_4 dimers, providing insight into ion cluster formation.

I. INTRODUCTION

Electrospray thrusters are a type of electrostatic propulsion system which are a competitive choice for use on small spacecraft due to their ability to efficiently produce charged particles at low powers[1], enabling the efficient acceleration to specific impulses of between 100 and 5000 seconds[2–7]. With the rise to prominence of small satellites[8], the need to continue the development of low power propulsion has become increasingly important, with electrospray thrusters being one of the most promising options.

Electrospray thrusters utilise the electrospray effect, which is achieved by applying a strong electric field to the surface of a liquid, distorting the surface of the liquid and, at a sufficiently high electric field strength, emits charged particles. The strong electric field is enabled by an electrospray thruster's two basic components, the emitter and the extractor. The emitter is a needle-shaped object with a high electric field promoting sharp tip, while the extractor is a thin metal plate with an aperture through which ions can be emitted. In order to produce the electric field the emitter is typically at a high voltage with the extractor grounded.

The electrospray effect can produce a large range of different charge-to-mass ratio charged particles based on the design of the electrospray thruster. However, high charge-to-mass ratio charged particles, called ions or ionic clusters, are typically desired because high charge-to-mass ratios lead to high exhaust velocities, v_{ex}. This can be shown by the equation,

$$v_{ex} = \sqrt{\frac{2(ne)\phi}{m}}, \tag{1}$$

where n is the amount of charge in a charged particle, e is the elementary charge of an electron, ϕ is the potential which the charged particles are accelerated by and m is the molecular mass of the charged particle. However, although this increases the specific impulse, the thrust, which is inversely proportional to the charge-to-mass ratio, will reduce as the charge-to-mass ratio increases. The reduction in thrust due to a higher charge-to-mass ratio can be offset by an increase in the total current emitted by the thruster, albeit with this increasing the total power used by the system. A comprehensive understanding of the ionic cluster emission mechanism, especially the factors affecting the charge-to-mass ratio of emitted ionic clusters and the current, is therefore imperative to design electrospray thrusters well.

One factor enabling the pure emission of ionic clusters from an electrospraying device is the use of certain room temperature molten salts, typically called 'Ionic Liquids', which are comprised of a cation and an anion, with the cations and anions being molecular. The molecular nature of these ions means that the number of combinations suitable for an ionic liquid is virtually limitless (up to 10^{18} combinations[9]!), potentially allowing for the creation of tailor made ionic liquids for different requirements of electrospray propulsion systems. Tailor made propellants would allow a single electrospray thruster design to be applicable to many different spacecraft requirements as operating on a suitably selected propellant would produce different sized ionic clusters and different currents, therefore different specific impulses and thrusts. This varying performance with different propellants would reduce the costs and time required to make new thrusters for different

[a)]Szymon.Dworski@soton.ac.uk
[b)]C.N.Ryan@soton.ac.uk

applications.

In practise requirements brings the number of ionic liquids suitable for electrospray thrusters to tens or hundreds. These requirements are typically that the thruster will emit adequate amounts of current to enable a suitable thrust level and emit charged particles with a suitable charge-to-mass ratio to produce a high enough specific impulse. The value for the current requirement varies with the geometric properties of the emitter and the application. Similarly, the specific impulse required will vary with the application of the thruster, with an example of a required specific impulse being greater than 1500 seconds[10].

The properties of these ionic liquids can have a significant effect on the performance of a thruster. Previous results have shown that ionic cluster emission can be significantly affected by the properties of these ionic liquids[11–13] but also shown to not have a significant effect on certain types of electrospray thrusters[14,15], with the influence of propellant properties seeming to be especially diminished when ionic clusters form the majority or entirety of a plume. One consistent trend is that the conductivity of the ionic liquid increases the current across literature[14,15], meaning a high conductivity propellant is typically desirable.

The complicated and at times somewhat contradictory nature of the effect of propellant properties, and the general availability of EMI-BF_4, has led to a large portion of recent electrospray thruster research utilising EMI-BF_4 for testing, as EMI-BF_4 generally ensures adequate thruster performance. However, with many possible ionic liquids, it would seem that the lack of predictability of performance of electrospray thrusters impedes the application of ionic liquids to electrospray thrusters. This has led our group at the University of Southampton to investigate the ion emission of different ionic liquids in order to understand the effects of various liquid properties on thruster performance, with a focus on investigating the size of ionic clusters emitted.

The ionic liquids selected in this study were based on more unconventional properties of ionic liquids, as opposed to the typical ionic liquid properties such as conductivity, viscosity and surface tension. The property of interest was the charge of either the cation or anion in the ionic liquid, specifically increasing the charge of the cation or anion, with a representation of this in Fig. 1. This group of ionic liquids was termed 'Multiply charged Ionic Liquids' (MILs).

One of the reasons for choosing these types of liquids was due to the effect the extra ion charges may have on the kinetics of the ion emission process. In electrospray ion emission an ionic cluster becomes energetic enough to overcome its energy barrier for emission, which is called the ion solvation energy ΔG[16]. This energy is made up of two components, the chemical energy required to be overcome due to inter-molecular bonding, ΔG_s^o, and a reduction in the energy required to evaporate due to the presence of a strong electric field, ΔG_e. This can be represented by the equation:

$$\Delta G = \Delta G_s^o - \Delta G_e. \tag{2}$$

Significant ionic cluster evaporation from the surface of a liquid typically occurs when $\Delta G_E \approx \Delta G_s^o$, corresponding to a very strong electric field, of the order of 1 V/nm. Under the electric field, the liquid forms a mensciscus of a conical shape, with a meniscus tip radius of approximately 10 - 100 nm[17]. ΔG_e can represented using the image charge model[18]:

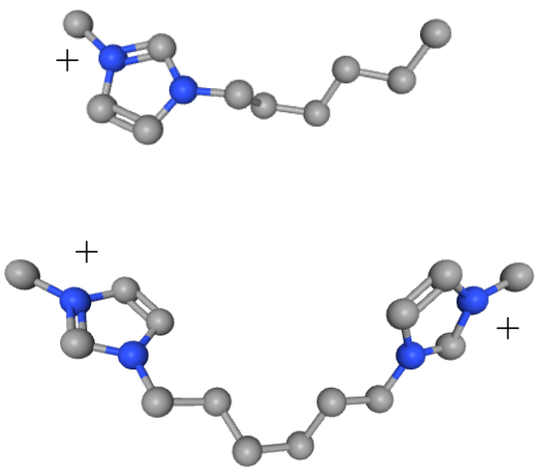

FIG. 1. Two ions, on the top is 1-Hexyl-3-methylimidazolium and on the bottom is 1-Methyl-3-[6-(3-methylimidazol-3-ium-1-yl)hexyl]imidazol-1-ium. The ions are of a very similar structure, except that the bottom ion has two imidazolium group, represented by the two pentagons, doubling the charge of the ion as opposed to the top ion with only a slight increase in mass. Both of these diagrams can found at *https://pubchem.ncbi.nlm.nih.gov/* by searching the stated chemical names.

$$\Delta G_e = \sqrt{\frac{(ne)^3 E}{4\pi\varepsilon_0}}, \tag{3}$$

where E is the normal electric field at the tip of the emitter and ε_0 is the permittivity of free space. Equation 3 shows that $G_e \propto (ne)^{\frac{3}{2}}$, which suggests that increasing the charge on the emitted ion should reduce the energy required for ion evaporation for a given intermolecular bonding strength, leading to a higher current and potentially higher charge-to-mass ratio ionic clusters being emitted by the electrospray thruster

A point will also be made here about ΔG_s^o. It is not clear how this quantity will scale with an increase in the charge of the ion. An exact experimental value for this number is not found in literature, although a value of 1-2 eV is typically accepted[17]. One way to estimate this value is by using the Born equation[19]:

$$\Delta G_s^o = \left(\frac{27\pi}{4}\right)^{\frac{1}{3}} \frac{\gamma^{\frac{1}{3}}(ne)^{\frac{4}{3}}}{(4\pi\varepsilon_0)^{\frac{2}{3}}} \left(1 - \frac{1}{\varepsilon}\right)^{\frac{2}{3}}, \tag{4}$$

TABLE I. The propellant properties of the three liquids tested. The MILs tested showed lower conductivities and significanty higher viscosities than EMI-BF_4.

Ionic Liquid	Conductivity, mS/cm	Viscosity, cP[a]	Surface Tension, mN/m	Cation mass, AMU[b]	Anion Mass, AMU
EMI-BF_4	14.6	33.8	52.0[20]	111.17	86.81
$(EMI)_2$-$Co(SCN)_4$	3.42	225	56.0[21]	111.17	291.30
$C_6(mim)_2$-$(IM)_2$	0.42	$\sim$ 590[22]	40[23]	248.30	281.16

[a] Unless cited, the viscosities were obtained from Iolitec GmbH.
[b] Cation and Anion masses were obtained from PubChem, *https://pubchem.ncbi.nlm.nih.gov/*

where ε is the relative permittivity of the solution. Equation 4 suggests that the energy barrier for emission scales with $(ne)^{\frac{4}{3}}$, increasing at a lower rate than the reduction in energy required for evaporation. For a given electric field and ionic liquid, Equations 3 and 4 would therefore suggest that a higher charge ion would decrease the barrier for ion evaporation more and therefore promote emission, making MILs an energetically attractive ionic liquid for ion evaporation.

However, the applicability of this equation to ionic liquids is uncertain, with the approximation being valid for ions in solution with previous attempts at utilising this equation not reproducing experimental data[24]. The Born approximation is typically used for approximating the energy of heavily diluted ions solvating from a dielectric medium, which is not a good description of ion emission from ionic liquids[25]. Therefore although the these equations suggest MILs may be an attractive group of ionic liquids for higher current and high charge to mass ratios, experimental evaluation is required. The testing of these ionic liquids will also expand the understanding of the ion emission process by showing what sorts of plumes are produced by two unconventional ionic liquids, adding to the previously tested ionic liquids in literature.

II. EXPERIMENTAL APPROACH

To investigate the effect of increasing the charge state of ionic liquids, two different MILs were identified alongside EMI-BF_4, which was used in the experiment as a control liquid. An experimental setup was created for testing which allowed for current collection, Retarding Potential Analysis (RPA) and Time-of-Flight Mass Spectrometry (TOF). Current collection was used to measure the total beam current produced by the thruster. RPA allowed for the identification of ions through field-free fragmentation[26], which importantly is based only on the mass as opposed to the charge to mass ratio. Finally, TOF allows for the identification of ion charge to mass ratios, $\frac{q}{m}$ and therefore the ionic cluster types for each propellant.

A. Ionic Liquids

The two multiply charged ionic liquids were selected primarily based upon availability, sourced from Iolitec GmbH. The first of these ionic liquids was bis(1-ethyl-3-methylimidazolium) tetrathiocyanatocobaltate, $(EMI)_2$-$Co(SCN)_4$, made up of two 1-ethyl-3-methylimidazolium cations and a doubly charged tetrathiocyanatocobaltate anion. The second MIL was 1,6-bis(3-methylimidazolium-1-yl)hexane bis(trifluoromethylsulfonyl)amide, $C6(mim)_2$-$(IM)_2$, made up of a doubly charged 1,6-bis(3-methylimidazolium-1-yl)hexane cation, shown in the bottom of Fig. 1, and two bis(trifluoromethylsulfonyl)amide anions.

The propellant properties that are known for these ionic liquids have been shown in Table I. All the ionic liquid conductivities were measured before testing using a Horiba LAQUAtwin-EC-33 condctivity meter, otherwise the source for the property is cited.

B. Electrospray Source and Emitters

The porous electrospray source used a single porous emitter, which was designed by Turan, Ma and Ryan[27]. The emitters were manufactured using CNC machining, made from P5 porous borosilicate glass sourced from ROBU, with a pore size pore size of 1.0 - 1.6 µm. Due to the manufacturing process of the emitters, there was some variation in the tip radii of the emitters. To take into account the effects of the varying emitter tip radii, an Alicona Infinitescan profilometer was used to accurately measure each emitter's geometrical properties. A typical scanned emitter can be seen in Fig. 2. A list of the tip radii for each emitter used and the liquid the emitter was used with can be found in Table II, with a typical emitter radius being 110 µm. Emitters 1 and 15 had a significant deviation in tip radii from emitters 2, 6 and 10 meaning that the current-voltage data could be somewhat affected by these tip radii differences. However, it is assumed that the TOF data, and also RPA data, will not be significantly affected by the tip radii based on previous experimental work various tip radii using externally wetted emitter tips[28].

The body of the thruster was manufactured from PEEK and with the design inspired by the AFET thruster[4]. The emitter to extractor distance was kept to approximately 100 µm for each test. The liquid reservoir was manufactured from porous stainless steel sourced from AmesPore, with a porosity of 51% and pore sizes from 39 to 83 µm. The liquid reservoir was waterjet cut from a sheet of porous steel.

TABLE II. The tip radii and heights of different emitter tips used in testing.

Emitter Number	Liquid	Radius (µm)	Height (µm)
2	EMI-BF_4	108.1	2070
1	$(EMI)_2$-$Co(SCN)_4$	124.9	2073
10	$(EMI)_2$-$Co(SCN)_4$	110.7	2045
6	$C_6(mim)_2$-$(IM)_2$	111.9	2231
15	$C_6(mim)_2$-$(IM)_2$	61.2	2067

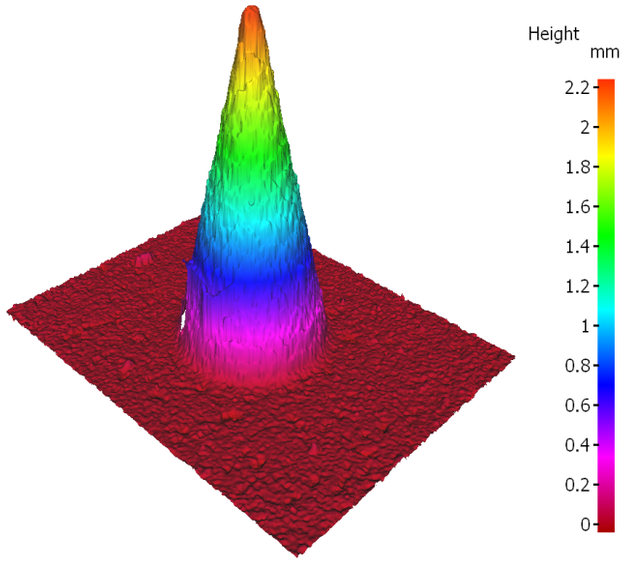

FIG. 2. A scan using the Alicona profilometer showing the conical shape of the emitter. This emitter had a tip radius of ~ 61 µm.

C. Apparatus

The tests were conducted at the David Fearn Electric Propulsion labratory at the University of Southampton in the 'Hatch' chamber. The background pressure that the chamber could reach was at minimum 7.4×10^{-7} mBar, however a typical pressure for testing was $\sim 1 \times 10^{-6}$ mBar. The pumps used were a dry scroll roughing pump and a turbo molecular pump.

In order to rapidly test different electrospraying devices and ionic liquids, a testing setup was built called the Porous Electrospray Thruster Rotating Testing Setup (PET-RTS). The aim was to allow the four main tests for electrospray thrusters (current collection, plume angle analysis, RPA and TOF) to be able to be conducted within a single pump-down of the chamber. This enabled more rapid testing of electrospraying devices and also increased reliability of tests due to the effect of moisture absorption by the ionic liquids, which tend to be hygroscopic, being negated between tests. A schematic of the system can be seen in Fig. 3.

The thruster was mounted on a Velmex V-B4872TS-BK rotary stage. The rotary stage allowed for rotation between the current collector, RPA and TOF after the chamber was pumped down, allowing all three tests to be conducted during one chamber pump down. The rotation was controlled by a LabVIEW program which allowed for positional control with an accuracy of 0.1^o.

The current collector is typical of collectors used in electrospray thruster research, with it being made from a 200 $\times$ 200 mm aluminium plate. Two grids were placed in front of it, spaced by 5 mm, with the closest grid to the collector plate being a secondary electron suppression grid with an applied voltage of -30 V and the farthest grid being a grounded grid. The grids were sourced from Precision Eforming and made from MN20 material, with a transparency of 88%. The collector current was measured by a FEMTO DHPCA-100 'Fast amp' (this was also used for RPA and TOF testing) which outputted the reading to a National Instruments DAQ system, where the data was collected and stored. The extractor current was measured by connecting the extractor to ground through a 100 kΩ resistor to ground, with the voltage across the resistor being measured by a digital multimeter.

The retarding potential analyser was an FC-72 purchased from Kimball Physics. The SEE voltage was -30 V, supplied by a desktop power supply. The retarding voltage for it was provided by a Matsusada AMT-5B20 power supply, with the power supply controlled by the LabVIEW program. The waveform had an 8 second rise time, with the fully repelling voltage held for 4 seconds.

Finally the TOF system consisted of a 'reflecting' electrostatic gate and a large metal collector plate. The 'reflecting' electrostatic gate had a voltage of +/- 3.49 kV applied to it by a DEI PVX-4140 pulse generator. For TOF, the gate voltage always exceeded the voltage that the ions were accelerated by. The gate has three electrodes, a central gate electrode where the potential was applied to and two grounded ones which were in front and behind the gate electrode with respect to the electrospray source. The flight distance between the gate and the collector, L, was 550 mm. The collector plate was a large metal collector plate with two grids similar to the collector plate. The first grid, which was offset by 5 mm from the surface of the collector, was the second electron suppression grid which had an applied voltage of -45 V provided by five 9 V batteries. The second grid, offset 5 mm from the secondary electron suppression grid, was grounded and ensured the potential would not leak into the flight path. The grids were made from the same material as the the collector plate grids. The current was recorded and averaged by a Wavesurfer 3024 oscilloscope. The gate signal was controlled by the LabVIEW program which ensured that the gate signal operated during bipolar thruster operation.

D. Methodology

This subsection will discuss the procedure of preparation and testing of the ionic liquids. To minimise extraneous effects on the ionic liquid and therefore ensure the reliability of the results, two key steps were taken in the preparation for testing. Firstly, all the ionic liquids were hygroscopic to a certain degree, and therefore in preparation for testing the propellant could absorb a significant amount of water before testing. In preparation for testing, the propellant was stored

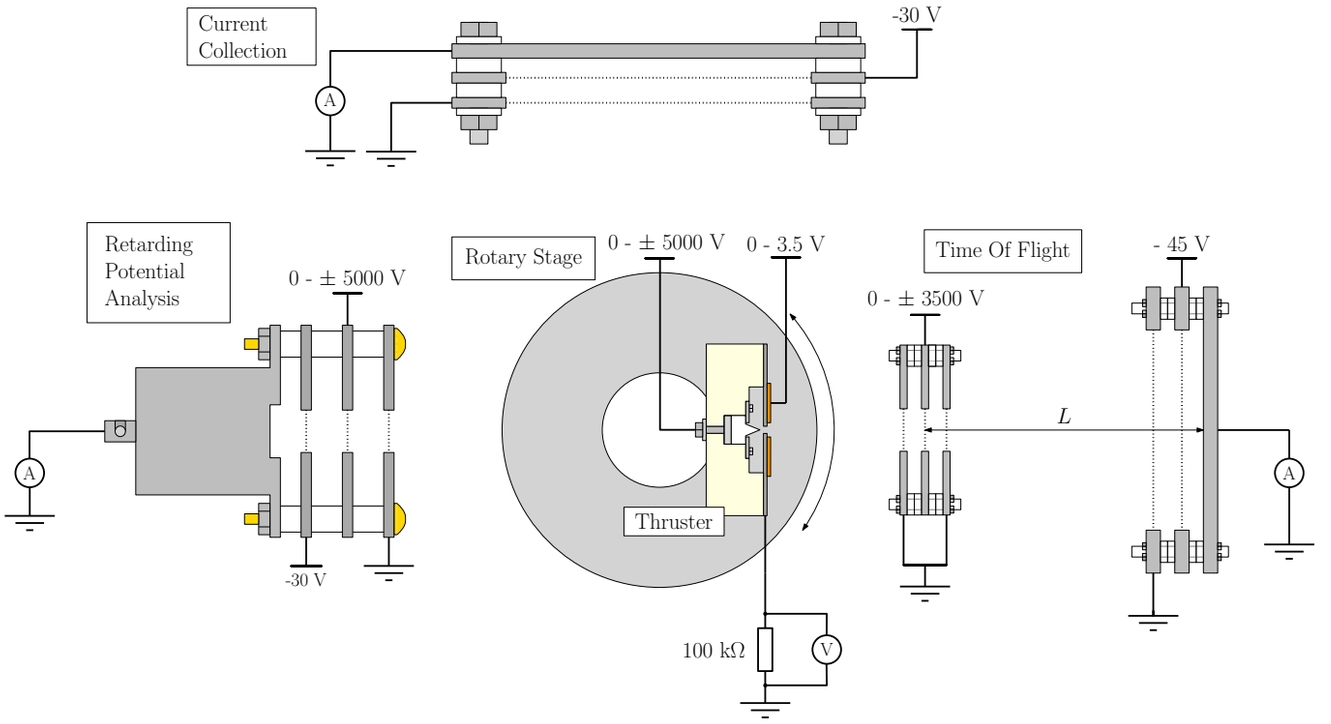

FIG. 3. The PET-RTS with the porous electrospray source mounted on the rotary stage. Three tests are conducted with each liquid: current collection, retarding potential analysis and time of flight. The respective diagram of each of the instrments is shown here with their electrical connections.

in vacuum for at least one day, to reduce any moisture within the propellant. When preparing the electrospray source, the time to complete the preparation between opening the vacuum chamber to atmosphere and pumping down the vacuum chamber was ~ 1 hour which minimised the ionic liquid's interaction with the atmosphere, in order to minimise the moisture content within the propellant. Furthermore the assembled electrospray source was placed inside of the chamber, pumped down and left overnight to allow for a final reduction of moisture before testing.

To minimise the cross contamination of ionic liquids, each electrospray source component was cleaned using isopropanol and an ultrasonic bath in between testing. The cleaning process included the liquid reservoir and the components were left to dry in atmosphere for approximately one hour for each test. For each test a new emitter was used. The ionic liquid was fed to the emitter and liquid reservoir with a pipette, with a new pipette being used for each test.

Once the electrospray source was ready to test in vacuum, it was pre-fired for between half an hour to an hour. It was found that the electrospray source would not emit as much current and would onset at a higher voltage until after it has been pre-fired. It is unknown precisely why this was the case however it was reported on in previous porous electrospray thruster experiments[5].

After pre-firing the electrospray source, the current was collected. The voltage was swept from the electrospray source's onset voltage, V_{onset}, to $V_{onset} + 1000$ V in order to observe how the ionic liquid would perform at higher voltages with respect to the electrospray source's onset voltage. The electrospray source was operated in a bipolar mode, with a square wave of frequency typically around 0.2 Hz. The extractor current was also collected during the current collection tests.

Once the current collection experiments were done, the electrospray source was rotated to the TOF system in order to conduct TOF experiments. TOF was typically initiated at several hundred volts above onset, about $V_{onset} + 300$ V for each emitter, at which point a measurable amount of current could be observed on the TOF collector. The voltage would then be incremented in steps of 50 V up to at least 200 V above the starting voltage, therefore the range was typically $V_{onset} + 300$ V to $V_{onset} + 500$ V. Due to a lack of previous experimental data on the electrospraying of these ionic liquids, caution was exercised to not damage the emitter, which was the reason for not testing the emitter across its entire voltage range. An average of 500 TOF waveforms were taken to maximise the signal to noise ratio of the averaged waveform. A waveform of the gate noise was also taken without the thruster operating. The gate waveform was subtracted from the averaged waveform for each voltage to minimise the effect of the gate noise. Finally, the data was passed through a low-pass 3rd order Butterworth Filter with a cut-off frequency of 5 MHz to reduce high frequency noise.

At the end of testing, retarding potential analysis was also conducted. Eight RPA curves were taken for each voltage, with the voltages taken at the same voltages as the TOF test-

ing. These were then averaged and a Savitzky-Golay filter was added to produce the final RPA graphs. It will be noted that the negative RPA data had constant negative gradient starting from onset voltage for all the ionic liquids tested, however this did not affect the identification of ion fragmentation.

III. RESULTS

A. Current

The current against voltage is shown in Fig. 4. The Figure shows five different tested emitters, one for EMI-BF_4, two for $(EMI)_2$-$Co(SCN)_4$ and two for $C_6(mim)_2$-$(IM)_2$. In the positive polarity the onset voltages were similar for all three propellants with $(EMI)_2$-$Co(SCN)_4$ having the lowest onset voltage and $C_6(mim)_2$-$(IM)_2$ having the highest. In the negative polarity the ionic liquids have a similar onset voltage as well, with both $(EMI)_2$-$Co(SCN)_4$ and EMI-BF_4 having very similar onset voltages, with $C_6(mim)_2$-$(IM)_2$ having the highest onset voltage.

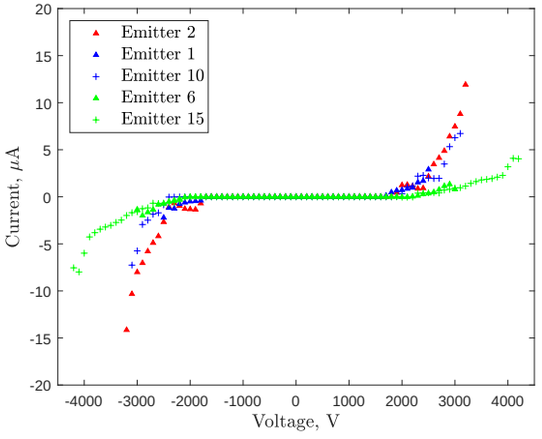

FIG. 4. The current against voltage for the ionic liquids . The colours represent the following liquids: EMI-BF_4 - red, $(EMI)_2$-$Co(SCN)_4$ - blue, $C_6(mim)_2$-$(IM)_2$ - green, with the details of emitters found in Table II.

Interestingly, it would be expected that the onset voltages would increase in order of their surface tensions[28], $V_{onset} \sim \gamma^{\frac{1}{2}}$, with $C_6(mim)_2$-$(IM)_2$ having the lowest onset voltage with EMI-BF_4 having 1.16 times higher and $(EMI)_2$-$Co(SCN)_4$ having 1.18 times higher onset voltage. This trend is not seen in the data with the high surface tension propellants onsetting at a lower voltage than the lowest surface tension propellant, $C_6(mim)_2$-$(IM)_2$. Furthermore, in terms of the onset voltage, the doubly-charged nature of the propellants does not seem to provide any benefits, with the onset voltages being explained by the surface tensions of the ionic liquids. However it will be noted that although the radii of the emitters were kept approximately the same, with the exception of emitter 15, there could be emitter effects which produce the onset voltage

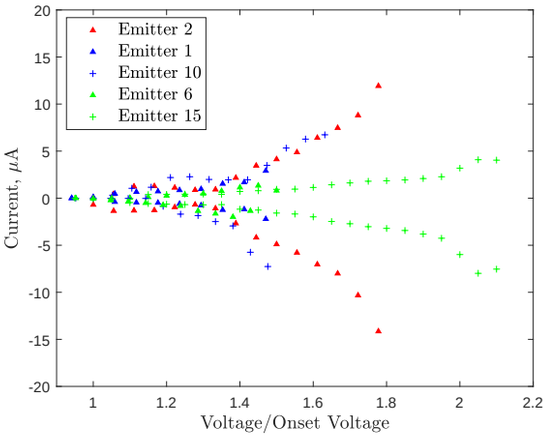

FIG. 5. The current emitted by liquid with the voltage being normalised to the source's onset voltage .

trend. Further experimentation with a focus on the onset and current emit is required in order to validate this conclusion.

To investigate the effect the doubly charged nature of the ions had on the current emitted by the ionic liquid, the onset voltage was normalised and the current data was plotted on Fig. 5. The three different ionic liquids are shown to have emitted different levels of current, with the most current being emitted by EMI-BF_4 followed by $(EMI)_2$-$Co(SCN)_4$ and $C_6(mim)_2$-$(IM)_2$, which is consistent with the conductivities of the ionic liquids, with EMI-BF_4 having the highest conductivity of 14.6 mS/cm. However, interestingly the rate at which the current increased was similar for EMI-BF_4 as with $(EMI)_2$-$Co(SCN)_4$ even though $(EMI)_2$-$Co(SCN)_4$ has a conductivity 4 times less than EMI-BF_4 and a viscosity of about 6.7 times more. This seems to provide an indication that the double charged of the molecule could be increasing the current emitted by the ionic liquid, more than if only simple ionic liquid properties are considered.

We will provide two final notes on the current data. Firstly, when the electrospray source operated using $(EMI)_2$-$Co(SCN)_4$ it had a tendency to spark preventing the emitter from operating. Although it is possible that the other two propellants sparked, it was especially pronounced for $(EMI)_2$-$Co(SCN)_4$. For any reader wishing to test the propellant, we would advise operating the thruster conservatively during testing. Secondly, although $C_6(mim)_2$-$(IM)_2$ emitted the least current, it was surprising that the electrospray source was able to emit over 5 μA in the negative polarity. The emission remained very stable even at higher voltages which was not expected and after the experiment the emitter was found to be identical in appearance to the emitter prior to testing, further suggesting a stable emission with little sparking and possibly few electrochemical reactions at this high voltage and relatively high current regime. This high voltage stability could mean that although the ionic liquid is not effective compared to, for example, EMI-BF_4 at lower voltages, it could be useful for applications requiring a high voltage.

B. Retarding Potential Analysis and Time-of-Flight

For the analysis of the RPA data in this study, only field-free fragmentation was considered to aid in the identification of certain ionic clusters. A more complete text on fragmentation which includes discussion about acceleration region fragmentation in porous electrospray sources can be found elsewhere[20,26].

The ions emitted by a porous electrospray source can be emitted in various clusters, with the simplest ionic cluster being a single cation or anion, for which the symbols A and B will be used respectively, similar to Larriba *et al*[24]. In this paper, singly charged cations and doubly charged cations (di-cations) were tested, which can be represented by A^+ and A^{2+} respectively. Similarly, singly charged anions and doubly charged anions (di-anions) were also tested, which can be represented by B^- and B^{2-} respectively. These ions can create clusters through bonding with neutral molecules, which are represented by AB. Therefore for a typical singly charged ionic liquid, the sizes of cations emitted are as follows: A^+, $A^+[A^+B^-]$, $A^+[A^+B^-]_2$, $A^+[A^+B^-]_3$ and so forth, with the names for these ions being 'monomers', 'dimers', 'trimers' and 'quadramers' respectively. The anion species would be similar, with the A^+ at the start of each ion being replaced by B^-.

When these clustered ions are emitted from the electrospray source, they can be unstable leading to break-up of the solvated species. This is true of all the ion cluster sizes except for monomers, which do not have anything to break up into, with the disassociation of individual molecules being unlikely due to the 'soft' ionisation nature of electrospray. As an example for a singly-charged cation dimer the fragmentation process would look as follows:

$$A^+[A^+B^-] \rightarrow A^+ + A^+B^-, \tag{5}$$

which describes a dimer breaking into a monomer and a neutral molecule. Similarly, a trimer fragmenting can be represented by the equation:

$$A^+[A^+B^-]_2 \rightarrow A^+[A^+B^-] + A^+B^-, \tag{6}$$

which describes a trimer fragmenting into a dimer and a neutral molecule. Equations 5 and 6 are typical fragmentations seen in electrospray sources. Other fragmentations are possible, with larger sizes fragmenting into a neutral molecule, and an ion with one less neutral molecule. Fragmentation with more than one neutral molecule being broken off are not typically seen in ionic electrospray plume data[29] and therefore will not be considered here.

Understanding the process of fragmentation, the energy changes caused by field-free fragmentation can now be analysed. Firstly, it is assumed that the energy is conserved during fragmentation. Secondly, the energy after fragmentation does not change as field-free fragmentation occurs outside of the electric field, therefore the collected ion energy will remain the same as the energy after fragmentation. Thirdly, the velocity of the ions remains constant throughout fragmentation. The kinetic energy of fragmentation can be described by considering that the an ion's variation in kinetic energy is proportional to the variation in electric potential energy[26],

$$q\phi_1 = \frac{1}{2}m_1{v_1}^2 \tag{7}$$

$$q\phi_2 = \frac{1}{2}m_2{v_2}^2, \tag{8}$$

where ϕ is the ion's potential, m is the ion's mass, v is the ion's velocity and the subscript $_1$ and $_2$ denote the energies before and after the fragmentation. The ratio of energies can be calculated by dividing Eq. 8 by 7,

$$\frac{q\phi_2}{q\phi_1} = \frac{m_2{v_2}^2}{m_1{v_1}^2}. \tag{9}$$

Since the fragmentation does not change the velocity, $v_1 = v_2$ and the charge does not change, therefore $q_1 = q_2$. Finally, it is assumed that the initial potential that the ion was accelerated by was by the potential of the emitter, therefore $\phi_1 = \phi_{emitter}$. Using these three assumptions, Eq. 9 can be rewritten as

$$\frac{\phi_2}{\phi_{emitter}} = \frac{m_2}{m_1}. \tag{10}$$

Equation 10 shows that the potential of field-free fragmentation can be determined by the ratios of masses of the ion before and after fragmentation. As an example, for a field free fragmentation of a cation dimer of EMI-BF_4 stopping potential of the fragmented ion would be determined by the ratio of A^+ to $A^+[A^+B^-]$, which is calculated as 0.360. What is important using this technique is that this energy is only dependent on the mass of the ions as opposed to the charge to mass of the ions. It will be noted here that when referring to the field-free fragmentation energy in the results section, it is in reference to ϕ_2.

Time-of-Flight mass spectrometry allows for the identification of the charge to mass ratios of ions emitted by the porous electrospray source. When an ion is emitted by the source, it is accelerated by the emitter potential to a velocity given by Equation 1. For TOF the time it takes for an ion to cross a specified length L is measured. The time it takes for an ion to cross this length can be described the equation $t = \frac{L}{v_{ion}}$, which when substituted with Equation 1 shows that the time it takes for an ion accelerated by a porous electrospray source is:

$$t = L\sqrt{\frac{m}{2q\phi_{emitter}}}. \tag{11}$$

Equation 11 can be further rearranged to describe the charge to mass ratio based on the time it takes for an ion to cross the TOF mass spectrometer:

$$\frac{q}{m} = \frac{L^2}{2\phi_{emitter}\,t^2}. \tag{12}$$

TABLE III. The various different types of ions calculated which could have been emitted by EMI-BF_4.

Ion Symbol	Simplified Representation	Chemical Formula	Charge to Mass Ratio, C/kg	Field Free Fragmentation Energy
α^0	A^+	EMI^+	8.67×10^5	Does not fragment
α^1	$A^+[A^+B^-]$	$EMI^+[EMI\text{-}BF_4]$	3.12×10^5	0.360
α^2	$A^+[A^+B^-]_2$	$EMI^+[EMI\text{-}BF_4]_2$	1.90×10^5	0.610
α^3	$A^+[A^+B^-]_3$	$EMI^+[EMI\text{-}BF_4]_3$	1.37×10^5	0.719
β^0	B^-	BF_4^-	-1.10×10^6	Does not fragment
β^1	$B^-[A^+B^-]$	BF_4^- $[EMI\text{-}BF_4]$	-3.38×10^5	0.305
β^2	$B^-[A^+B^-]_2$	BF_4^- $[(EMI\text{-}BF_4]_2$	-2.00×10^5	0.590

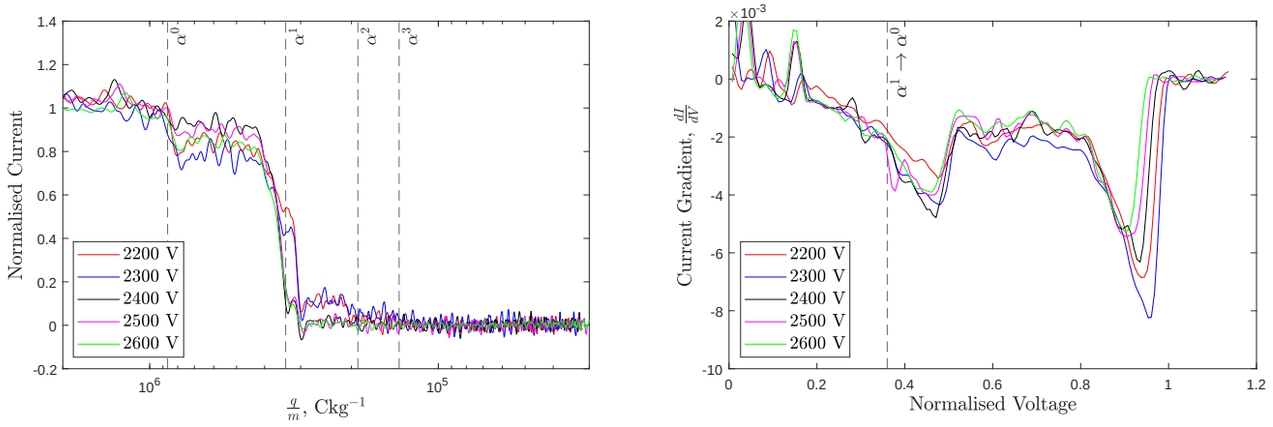

FIG. 6. Positive polarity TOF and RPA data for emitter 2 using EMI-BF_4.

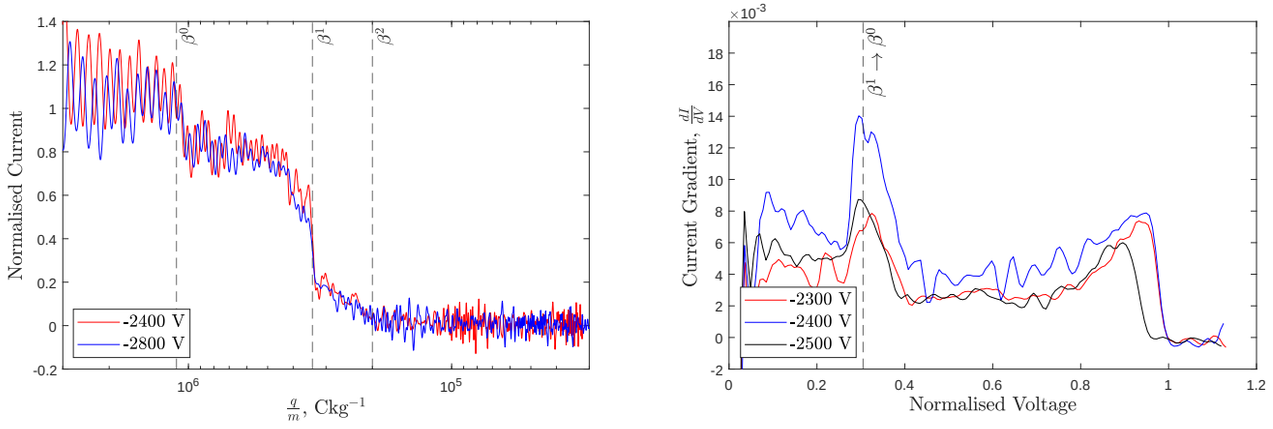

FIG. 7. Negatve polarity TOF and RPA data for emitter 2 using EMI-BF_4.

Equation 12 is used to transform the raw current against time TOF data to current against the charge to mass ratio.

Finally, for both of these data sets, the current was normalised by the current at no retarding voltage for RPA and the current at the time which the monomers arrive for TOF. This allows for easier comparisons of the data with the voltage change, which typically increases the current. Furthermore, for the RPA data the voltage was normalised with the emitter voltage.

1. *EMI-BF_4*

The first TOF and RPA data that will be presented are the EMI-BF_4 data in order to produce a baseline data set for the types of ions are emitted from the most common ionic liquid

used in electrospray sources (EMI-BF_4). Figure 6 shows the positive polarity TOF and RPA data for emitter 2. The TOF data show a range of ion species emitted by the electrospray source, with the species emitted being monomers, α^0, dimers, α^1, trimers, α^2, and quadramers, α^3. The properties of each ion can be seen in Table III. The data were quite noisy as although EMI-BF_4 emitted a lot of current, a large proportion of the current did not reach the TOF collector therefore making accurate descriptions of the proportions of each ion difficult. However, this does not significantly impede the ability to identify the ions that are in the plume.

The species seen are typical of what is expected from an ionic liquid electrospray source using EMI-BF_4 emitting only ions. Typical EMI-BF_4 plumes emit mostly monomers and dimers, with some larger species also present[13,15,30]. The data show a plume which comprised primarily of dimers, with at certain voltages the plume comprises almost entirely of dimers such as at 2400 V, higher than what maybe expected with thrusters comprised of similar emitters and porous reservoirs[31,32].

The positive polarity RPA shown here provide supporting evidence for the species emitted by the electrospray source. The positive polarity RPA data is shown on the right hand side of Fig. 6. The axes show the differentiated current collected during the RPA experiment against the voltage normalised to the emitter voltage. The data show two distinct peaks at different normalised voltages, with the peak occurring at a normalised voltage of ~ 1 corresponds to ions accelerated the potential of the emitter tip, can be any emitted ion. The second peak occurring at a normalised voltage of ~ 0.4 seems to correspond to the fragmentation of a positive dimer, α^1, albeit at a slightly higher than expected energy. This fragmentation takes the same form as Equation 5, with a stopping potential of the ion calculated in Table III, 0.360, and is at a somewhat lower normalised voltage than the experimentally shown peak. The lack of other peaks appears to be in agreement with the TOF data, suggesting that the plume is comprised primarily of dimers, in agreement with the TOF data. Although these data show some instrumentation error with the energies being higher than the theoretical value, the other RPA data match well with the expected energy and therefore it remains unclear why these appear to be more energetic than expected.

The negative polarity data for the experiment were also taken, shown in Fig. 7. The TOF data is shown on the left hand side. The data show three drops in the current, corresponding to monomers, β^0, dimers, β^1, and trimers, β^2 being emitted by the electrospray source, shown on the figure using dashed lines. Due to a low signal, the TOF data is noisy, with the noise originating from the switching of the gate, however the species within the plume can still be identified. The species composition in the negative polarity is similar to the positive polarity which is typical of EMI-BF_4. Furthermore, similar to the positive polarity, the main species emitted in the negative polarity is a dimer.

The negative polarity RPA data, shown on the right hand side of Fig. 7, further support the plume is mostly comprised of dimers. Similar to the positive polarity, two prominent peaks can be seen, with the most interesting peak, around a normalised voltage of ~ 0.3, indicating the fragmentation of a negative dimer, β^1. This can be described by the fragmentation

$$B^-[A^+B^-] \rightarrow B^- + A^+B^-. \tag{13}$$

The two polarities shown here provide two predictions for the MIL TOF and RPA data. Firstly, it is expected that the thruster will operate in a purely ionic regime due to previous experiments with low conductivity showing purely ionic emission when used with a similar electrospraying system[14,15]. For the same reason, it is also expected that similar ions will be emitted from the electrospray thruster using the MILs meaning that the thruster will primarily emit monomers and dimers.

2. $(EMI)_2$-$Co(SCN)_4$

Figure 8 shows the TOF data when using $(EMI)_2$-$Co(SCN)_4$ for two different emitters, emitter 1 and emitter 10. Due to noise issues when testing emitter 15 in the positive polarity, only a single voltage had a sufficient signal to noise ratio during TOF. The dashed line on the figure represents the species identified to have been emitted, with the symbol corresponding to the ion shown in Table IV. In the negative polarity, the data show a sharp peak at around the charge to mass ratio of di-anion dimers, β^1, corresponding to a large proportion of the current ($\sim$ 80% - 90%) being comprised of them. The data show also the presence of di-anionic trimers, β^2, and quadramers, β^3, with a small to negligible amount of monomers, β^0, also shown.

The RPA data for both emitters are shown in Fig. 9. For both the emitters, it can be seen that, as with EMI-BF_4, the most prominent peak is around a normalised voltage of ~ 1, which corresponds to ions arriving at the RPA collector after being fully accelerated by the emitter potential. However, a second prominent peak can be seen around a normalised voltage of ~ 0.6. This peak corresponds to the field free fragmentation of a di-anion trimer fragmenting into a di-anion dimer, $\beta^2 \rightarrow \beta^1$, which corresponds to the fragmentation:

$$B^{2-}[2(A^+)B^{2-}]_2 \rightarrow B^{2-}[2(A^+)B^{2-}] + 2(A^+)B^{2-}. \tag{14}$$

It is interesting to contrast the TOF and RPA data with the EMI-BF_4 data, where significant amounts of monomers and dimers were emitted as well. The EMI-BF_4 RPA data showed a distinct fragmentation at a normalised voltage of $\sim$ 0.4, corresponding to dimer field-free fragmentation, whereas with $(EMI)_2$-$Co(SCN)_4$ for the negative polarity RPA data no evidence of field free dimer fragmentation is seen. Since the emitters had approximately the same geometric properties and the liquid reservoir was kept similar, this seems to suggest that some factor causes the di-ion to tend to emit more stable dimers as opposed to monomers. We propose here that this is likely due to the di-ion bonding stronger with the neutral than the singly charged ion[33]. This would explained the lack

TABLE IV. The various different types of ions calculated which could have been emitted by $(EMI)_2$-$Co(SCN)_4$.

Ion Symbol	Simplified Representation	Chemical Formula	Charge to Mass Ratio, C/kg	Field Free Fragmentation Energy
α^0	A^+	EMI^+	8.67×10^5	Does not fragment
α^1	$A^+[2(A^+)B^{2-}]$	$EMI^+[(EMI)_2\text{-}Co(SCN)_4]$	1.54×10^5	0.178
α^2	$A^+[2(A^+)B^{2-}]_2$	$EMI^+[(EMI)_2\text{-}Co(SCN)_4]_2$	8.46×10^4	0.549
β^0	B^{2-}	$Co(SCN)_4{}^{2-}$	-6.62×10^5	Does not fragment
β^1	$B^{2-}[2(A^+)B^{2-}]$	$Co(SCN)_4{}^{2-}$ $[(EMI)_2\text{-}Co(SCN)_4]$	-2.39×10^5	0.362
β^2	$B^{2-}[2(A^+)B^{2-}]_2$	$Co(SCN)_4{}^{2-}$ $[(EMI)_2\text{-}Co(SCN)_4]_2$	-1.46×10^5	0.610
β^3	$B^{2-}[2(A^+)B^{2-}]_3$	$Co(SCN)_4{}^{2-}$ $[(EMI)_2\text{-}Co(SCN)_4]_3$	-1.05×10^5	0.720
ζ^0	$2(A^+)$	$2(EMI^+)$	8.67×10^5	0.500
ζ^1	$2(A^+)[2(A^+)B^{2-}]$	$2(EMI^+)[(EMI)_2\text{-}Co(SCN)_4]$	2.61×10^5	0.302
ζ^2	$2(A^+)[2(A^+)B^{2-}]_2$	$2(EMI^+)[(EMI)_2\text{-}Co(SCN)_4]_2$	1.54×10^5	0.589

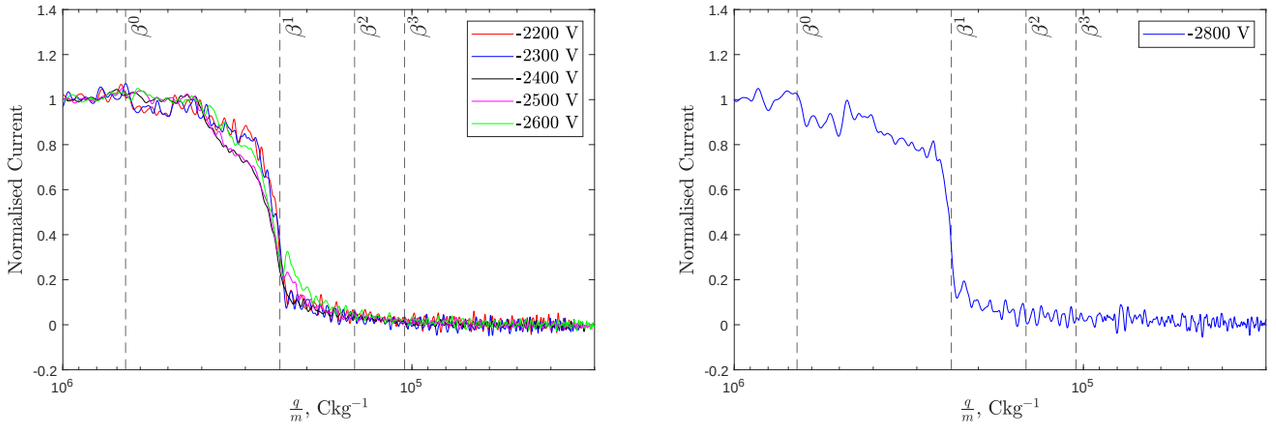

FIG. 8. Negative polarity TOF data for emitter 1, left, and emitter 10, right, using $(EMI)_2$-$Co(SCN)_4$.

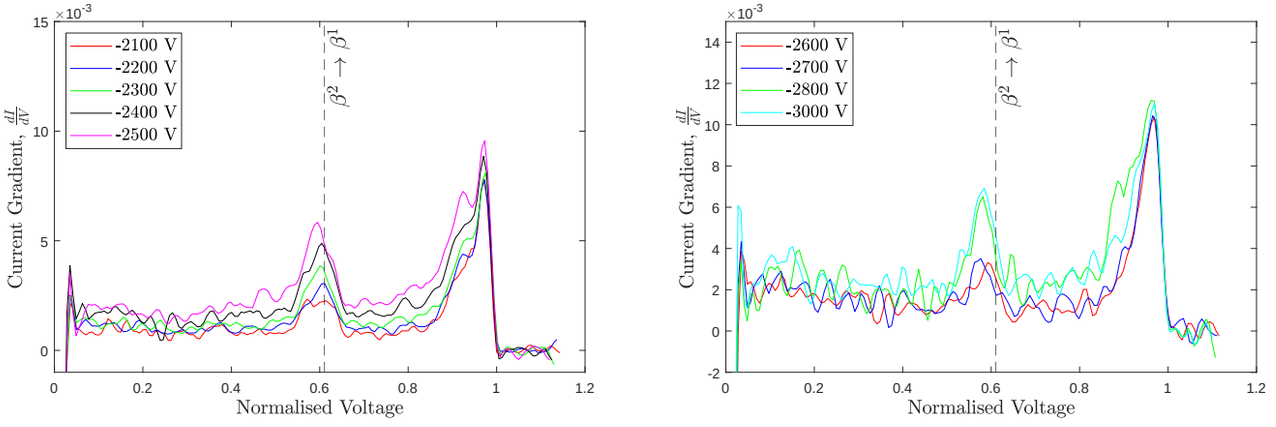

FIG. 9. Negative polarity RPA data for emitter 1, left, and emitter 10, right, using $(EMI)_2$-$Co(SCN)_4$.

of dimer field-free fragmentation in the RPA data of $(EMI)_2$-$Co(SCN)_4$ and the larger amount of dimers in the plume, possibly providing the first ion property which could be used for ionic cluster size prediction.

The thruster was also tested in the positive polarity, starting with the positive TOF data shown in Fig. 10. The data show three distinct drops, corresponding to three ionic species emitted. The species seemed to be similar to EMI-BF_4 in repre-

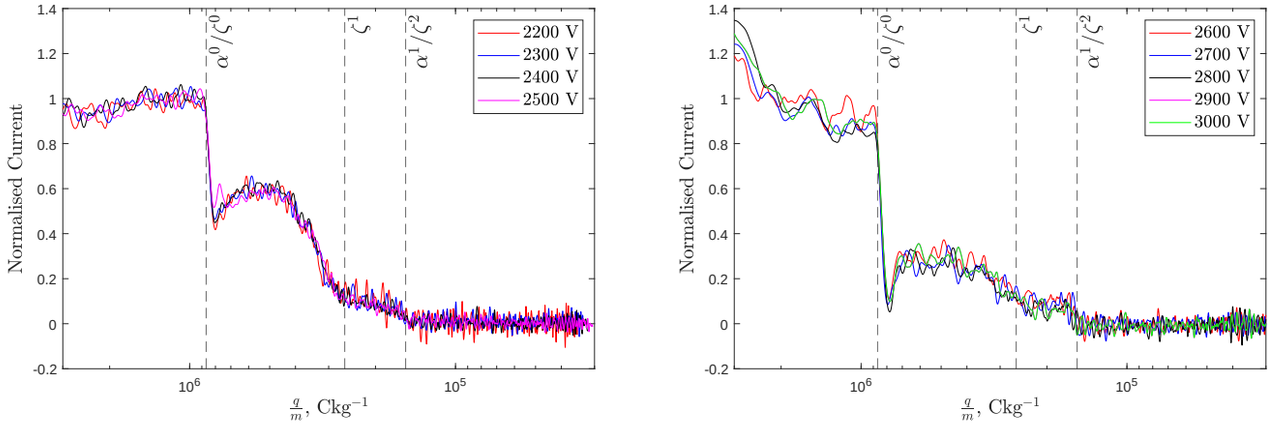

FIG. 10. Positive polarity TOF data for emitter 1, left, and emitter 10, right, using $(EMI)_2$-$Co(SCN)_4$.

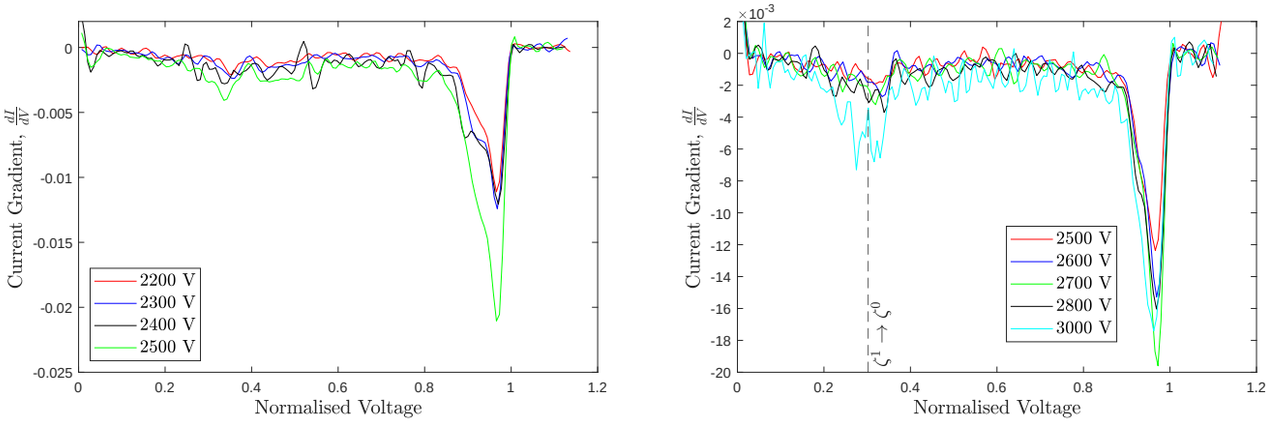

FIG. 11. Positive polarity RPA data for emitter 1, left, and emitter 10, right, using $(EMI)_2$-$Co(SCN)_4$.

senting monomers, dimers and trimers as opposed to the negative polarity emission using $(EMI)_2$-$Co(SCN)_4$. However, one major difference was in the species emitted, which can be seen plotted on the graphs using the dotted line. Initially it was predicted that the ionic liquid would emit species similar to EMI-BF_4, which denoted by the symbol α in Table IV. These would comprise of a single anion attached to a number of neutrals. However, although two possible drops were identified for both emitters which correspond to the α ions, the α^0 monomer and the α^1 dimer, there is a third drop in between the two which does not seem to correspond to any of the α ions. Although this could possibly be explained by fragmentation of the dimer into a monomer, the significant change in gradient and current at the drop in the data suggests that this is in fact a different ion species as opposed to fragmentation.

The solution which fit this data the best was to introduce a new species, ζ, which is comprised of a 'double cation', $2(A^+)$, as opposed to a cation, A^+. This naming is also used to distinguish the ions from di-anions and di-cations, B^{2-} and A^{2+} respectively. The 'double cation' ions have been given the symbol ζ, and their information can be found in Table IV. The current drops in the data well to a 'double cation' monomer, ζ^0, a dimer, ζ^1, and a trimer, ζ^2, which have been marked on Fig. 10 using a dashed line. There has been at least one other study by Gamero-Castaño and De La Mora[34] where a 'double ion' species was emitted using formamide and propanol doped with tetraheptyl ammonium bromide. However, this would be the first case that such a species was detected using only an ionic liquid. In the study by Gamero-Castaño and De La Mora, it was shown that both singly charged and doubly charged species were emitted by the thruster. This could also be the case with the data seen here with both the cation and 'double cation' monomer, α^0 and ζ^0, having the same charge to mass ratio and the cation dimer and 'double cation' trimer, α^1 and ζ^2, having the same charge to mass ratios.

Using the positive RPA data it is possible to distinguish which species were emitted based on the field free fragmentation reactions which occur in the plume. Fig. 11 shows the RPA data for emitter 1 and emitter 10. The emitter 1 data showed no significant peaks, other than around a normalised

voltage of 1, which represents non-fragmented ions arriving at the RPA collector. A slight peak can be seen at a normalised voltage of ~ 0.35, however this is interpreted as noise as opposed to evidence of field free fragmentation. However, the emitter 10 RPA data at voltage of 3000 V show a clear peak at a normalised voltage of ~ 0.302, likely corresponding to field free fragmentation of the double cation dimer, ζ^1. This has been marked on the plot with a dashed line. The fragmentation of the double cation dimer, ζ^1, can be represented by the equation

$$2(A^+)[2(A^+)B^{2-}] \rightarrow 2(A^+) + 2(A^+)B^{2-}. \quad (15)$$

This fragmentation corresponds well to the prevalence of double cation dimers in the TOF data, providing a strong argument for the data shown being explained by double cation emission.

However, the fragmentation of the double cation dimer also provides the largest source of uncertainty within this analysis of the data. This doubt originates from the fact that it would seem the most likely case that the double cation monomer, ζ^0, would be unstable and therefore break apart immediately after the fragmentation of the double cation dimer, which is described by the fragmentation

$$2(A^+) \rightarrow A^+ + A^+. \quad (16)$$

This fragmentation would appear as a peak at 50% of the energy of field free fragmentation of ζ^1, which would be a peak at a normalised voltage of 0.151. However, this peak is not seen in either of the emitters' RPA data. An alternative solution could be the the double cation dimer, ζ^1, fragments into a cation dimer, α^1, followed by the cation dimer fragmenting into a cation monomer, α^0. This fragmentation is described by the equations

$$2(A^+)[2(A^+)B^{2-}] \rightarrow A^+ + A^+[2(A^+)B^{2-}], \quad (17)$$

$$A^+[2(A^+)B^{2-}] \rightarrow A^+ + 2(A^+)B^{2-}. \quad (18)$$

The ions produced by this fragmentation would appear as a peak at the normalised voltages of 0.178 and 0.216 respectively. However, as with the fragmentation of the double cation monomer, no peaks are seen in the RPA data which seem to correspond to these two fragmentations. The consideration of these two alternate fragmentation scenarios, and their lack of evidence within the data, suggests that double cation monomers, ζ^0, are produced in the fragmentation of double cation dimers, ζ^1, and the double cation monomers emitted are stable.

3. $C_6(mim)_2$-$(IM)_2$

The $(EMI)_2$-$Co(SCN)_4$ test showed surprising results, which made it imperative to test a different MIL in order to investigate the ion bonding in MILs. $C_6(mim)_2$-$(IM)_2$ was therefore tested with it having it a di-cation as opposed to the di-anion of $(EMI)_2$-$Co(SCN)_4$. It also is the only MIL which has had some testing in electrospray propulsion[23]. The calculated ionic cluster sizes can be seen in Table V.

Figure 12 shows the negative polarity data for two emitters, emitter 6 and 15. Similar to $(EMI)_2$-$Co(SCN)_4$ the data show three, possibly four different species of ions. Initially, the single anion species, β, was fitted on the data to determine whether the data could be well explained by single anion ions. The single anion monomer, β^0, and single anion dimer, β^1, fit well with the data, as for the positive emission of $(EMI)_2$-$Co(SCN)_4$. However as with the positive emission data for $(EMI)_2$-$Co(SCN)_4$ a better fit can be achieved if a second 'double anion' species, ζ, is introduced. Both the different emitter data show that the emission of 'double anion' monomers, ζ^0, dimers, ζ^1, trimers, ζ^2, and possibly quadramers, ζ^3, correspond to the location for each significant current drop or change in gradient.

Figure 13 shows TOF data for Emitter 6 with a larger charge-to-mass ratio range which was undertaken a few months after initial tests with Emitter 6. The data show good agreement in the ionic clusters emitted by the the emitter, however a noticeable tail can be seen in the data, which corresponds to a population of droplets down to a charge-to-mass ratio of around 2×10^3 CKg^{-1}. This suggests that the emitter can emit larger ionic clusters as well as droplets, as opposed to the previously tested two liquids. It is unclear what could cause the emission of droplets as previous emitter 6 data indicating few large ionic clusters, with one possibility being that this test was conducted after the emitter was kept in storage for 8 months. Nonetheless, the data show a similar distribution of monomers, dimers and trimers with this plume being comprised primarily of ionic clusters, reinforcing the emission of double ion cations, ζ, emitted by the ionic liquid.

Figure 14 shows the negative polarity RPA data for emitter 6. The data show a distinct a peak at around a normalised voltage of ~ 1, corresponding to fully accelerated ions arriving at the collector. A second peak can be seen at a normalised voltage of ~ 0.3.

This voltage corresponds well to the fragmentation of a cation dimer, β^1, into a monomer, β^0. This fragmentation takes the form

$$B^-[A^{2+}2(B^-)] \rightarrow B^- + A^{2+}2(B^-). \quad (19)$$

The drop suggests that more typical dimers are emitted in the plume of $C_6(mim)_2$-$(Im)_2$, suggesting that potentially both types of ions, that is anions, β and 'double anions', ζ, can be emitted by a MIL, although further testing is required to verify the emission of the 'double ions'.

For emitter 6 using $C_6(mim)_2$-$(Im)_2$, the positive polarity TOF data are shown in Fig. 15. Unfortunately, the signal to noise ratio of the positive polarity data was too low for emitter 15 and therefore the data are not shown here for both TOF and RPA.. The data show a signal with a steep drop the charge to mass ratio expected for di-cation dimers, α^1, followed by a steady decrease in current corresponding to the presence of di-cation trimers, α^2, and quadramers, α^3. Due to noise it is

TABLE V. The various different types of ions calculated which could have been emitted by $C_6(mim)_2$-$(IM)_2$.

Ion Symbol	Symbol Representation	Chemical Formula	Charge to Mass Ratio, C/kg	Field Free Fragmentation Energy
α^0	A^{2+}	$C_6(mim)_2{}^{2+}$	7.76×10^5	Does not fragment
α^1	$A^{2+}[A^{2+}2(B^-)]$	$C_6(mim)_2{}^{2+}$ $[C_6(mim)_2\text{-}(IM)_2]$	1.87×10^5	0.241
α^2	$A^{2+}[A^{2+}2(B^-)]_2$	$C_6(mim)_2{}^{2+}$ $[C_6(mim)_2\text{-}(IM)_2]_2$	1.06×10^5	0.569
α^3	$A^{2+}[A^{2+}2(B^-)]_3$	$C_6(mim)_2{}^{2+}$ $[C_6(mim)_2\text{-}(IM)_2]_3$	7.44×10^4	0.699
β^0	B^-	Im^-	-3.43×10^5	Does not fragment
β^1	$B^-[A^{2+}2(B^-)]$	Im^- $[C_6(mim)_2\text{-}(IM)_2]$	-9.07×10^4	0.265
β^2	$B^-[A^{+}2(B^-)]_2$	Im^- $[C_6(mim)_2\text{-}(IM)_2]_2$	-5.23×10^4	0.576
ζ^0	$2(B^-)$	$2(Im^-)$	-3.43×10^5	0.500
ζ^1	$2(B^-)[A^{2+}2(B^-)]$	$2(Im^-)$ $[C_6(mim)_2\text{-}(IM)_2]$	-1.43×10^5	0.419
ζ^2	$2(B^-)[A^{2+}2(B^-)]_2$	$2(Im^-)$ $[C_6(mim)_2\text{-}(IM)_2]_2$	-9.07×10^4	0.632
ζ^3	$2(B^-)[A^{2+}2(B^-)]_3$	$2(Im^-)$ $[C_6(mim)_2\text{-}(IM)_2]_3$	-6.64×10^4	0.731

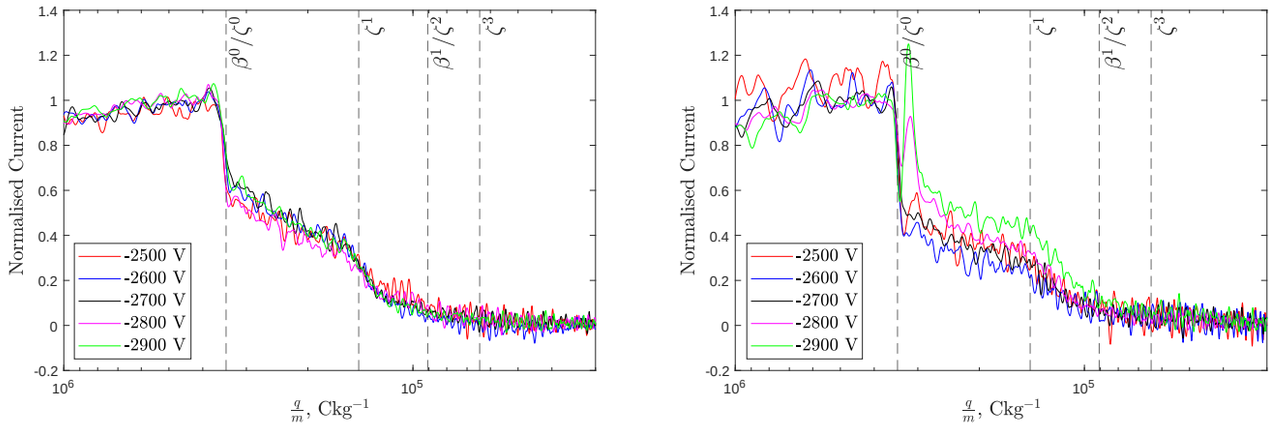

FIG. 12. Negative polarity TOF data for emitter 6, left, and emitter 15, right, using $C_6(mim)_2$-$(IM)_2$.

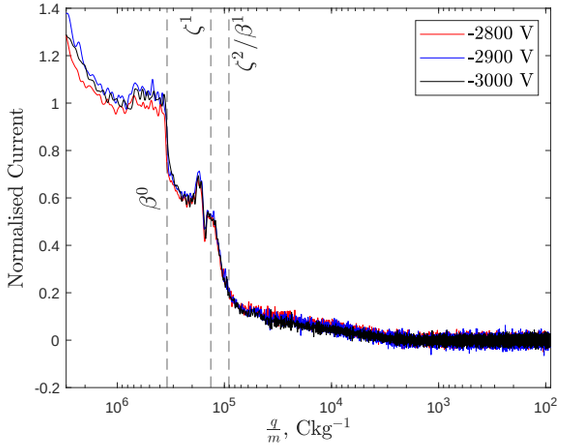

FIG. 13. Negative polarity TOF data for emitter 6 using $C_6(mim)_2$-$(IM)_2$ with a much broader range of charge-to-mass ratios.

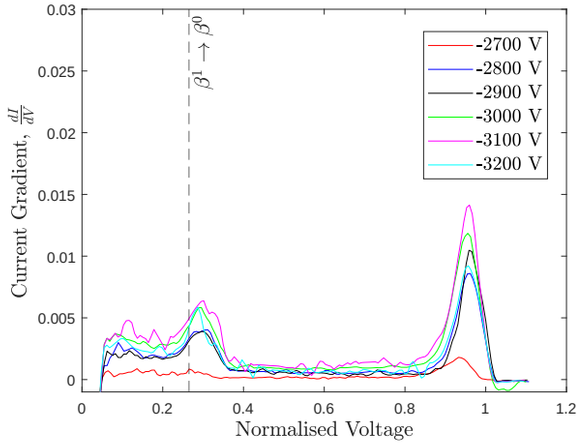

FIG. 14. The negative polarity RPA data for emitter 6, using $C_6(mim)_2$-$(IM)_2$.

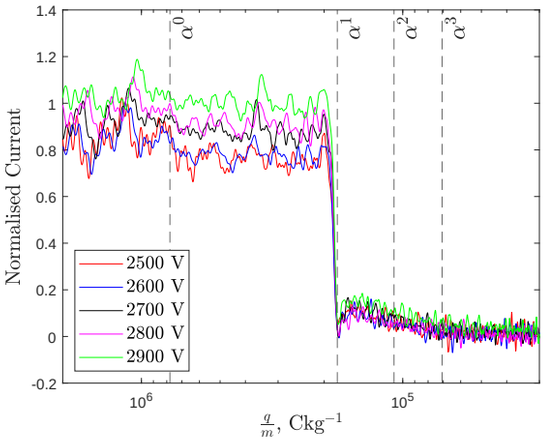

FIG. 15. Positive polarity TOF data for emitter 6, using $C_6(mim)_2$-$(IM)_2$.

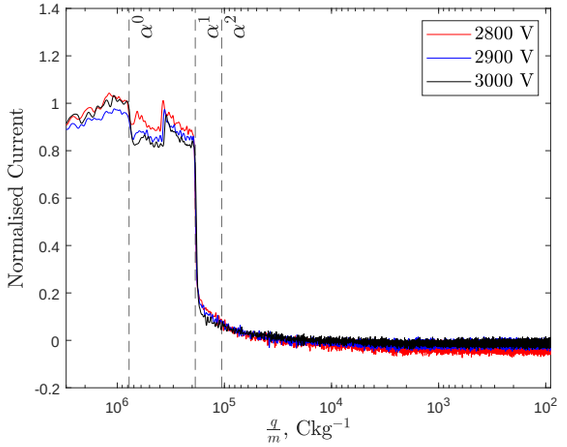

FIG. 16. Positive polarity TOF data for emitter 6 using $C_6(mim)_2$-$(IM)_2$ with a much wider range of charge-to-mass ratios.

unclear whether any di-cation monomers are present, however nonetheless the data show a plume comprised almost purely of dimers. As far as the authors are aware, an electrospray plume which emits such an almost purely dimer plume has not been reported before.

Positive polarity TOF data over a broader range of charge-to-mass ratios were also taken for this emitter, shown in Fig. 16. These data show a very similar plume to the data in Fig. 15, with a very sharp dimer drop representing up to 80% of the current, and a similar distribution of heavier ionic clusters, comprising up to 15% of the plume. The data show that the plume can be considered almost purely ionic, with a tail possibly extending to 2×10^3 Ckg^{-1}, suggesting some droplet emission. As with the previous longer period TOF data, these were taken after a long period of storage which may affect the distribution of ionic clusters emitted, possibly explaining the difference between the shorter and longer period data.

Positive polarity RPA data were also collected for emitter 6, shown in Fig. 17. The figure shows one strong peak at around the emitter voltage, corresponding to ions arriving at the collector after being fully accelerated with no other discernible peaks. The lack of any other peaks means that insignificant amounts of field-free fragmentation, possibly suggesting a higher stability of the ions emitted in the positive polarity, especially for the α^1 dimer.

As has been discussed with the $(EMI)_2$-$Co(SCN)_4$ data, it would seem that these data further suggest that the di-ion dimers bond stronger and are therefore more stable than the dimers produced by EMI-BF_4. This is both supported by the TOF and RPA data. The TOF data seem to show more dimers emitted for both of the di-ionic liquids suggesting a large amount of stable initial dimers. Field-free fragmentation appears in the $(EMI)_2$-$Co(SCN)_4$ data with the di-anion trimer fragmentation, however even with the abundance of dimers in the plume the RPA data show no evidence of dimer field free fragmentation. Therefore it seems that the TOF and RPA data of both the ionic liquids are better explained by a higher stability of the di-ion dimer. One of the possible reasons why these dimers could be more stable is the double charges of within the ions. The extra charge would allow for a much stronger electrostatic bond between the charges within the dimer, which would explain the both the lack of a dimer field-free fragmentation peak in the RPA data as well as the prominence of dimers throughut the TOF data.

The link between the strength of the bonding of the dimers and the relative amount of dimers in the plume seems to suggest that the bond strength of the ions could be a method to predict the sizes of ionic clusters between ionic liquids. This would be in sharp contrast to the bulk ionic liquid properties so far used to predict sizes of ionic clusters emitted, however it provides a new set of properties, the ion properties, to investigate as opposed to focusing only on bulk ionic liquid prop-

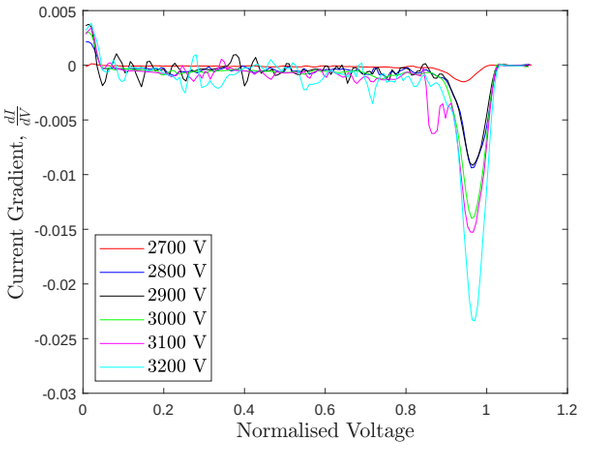

FIG. 17. The positive polarity RPA data for emitter 6, using $C_6(mim)_2$-$(IM)_2$.

erties.

IV. CONCLUSION

The current voltage, TOF and RPA data for three different ionic liquids, EMI-BF_4 and two MILs, $(EMI)_2$-$Co(SCN)_4$ and $C_6(mim)_2$-$(IM)_2$ were presented. The data have shown that the current emitting properties of the MILs seem more favourable than if only their liquid properties were compared due to the fact that $(EMI)_2$-$Co(SCN)_4$ emitted similar amounts of current to EMI-BF_4 even with a 4.3 times lower conductivity, a 6.6 times higher viscosity and 1.08 times higher surface tension, all properties which would contribute to a diminished current emission. Similarly $C_6(mim)_2$-$(IM)_2$ emitted relatively high currents of -7.5/+4.0 µA which are high considering a 34.8 times lower conductivity and approximately 17.5 times lower viscosity. This seems to suggest that the double charge of the ions within the molecule increases the effect of the electric field on the emission of ions.

The ions emitted by the MILs also support that the ionic liquid properties, especially conductivity and viscosity, do not provide a good way of predicting the sizes of ionic clusters emitted from an electrospray source when emitting only ions, with $C_6(mim)_2$-$(IM)_2$ being the only ionic liquid showing some larger ionic cluster and possibly droplet emission. This is in agreement with previous studies that have investigated the effects of ionic liquid properties on the sizes of ions in a purely ionic electrospray plume.

Furthermore, we believe the data suggest the emission of an interesting class of ions, termed 'double ions'. The data indicated that for the field free-fragmentation peaks in the RPA data for the $[EMI]_2$-$Co(SCN)_4$, the double ions, ζ, matched much better with the energies of these peaks than the expected α or β ions. Further investigation of MILs is required however in order to verify the emission of these ions. The existence of these ions might provide an insight into the ion formation in the meniscus of electrospray sources.

Finally, the dimers produced by the MILs within this study have been shown to be especially stable, with both the TOF data sets showing more dimers than EMI-BF_4 and the RPA data showing no indication of dimer field-free fragmentation for the MILs. The stability of dimers seem to promote the emission of dimers, showing evidence that ion properties, as opposed to bulk ionic liquid properties, provide a method of predicting the sizes of ionic clusters in electrospray ion emission. Further investigation of the chemical reasons of ion stability and further experimental investigation will be required to fully explore how ion stability affects the size of emitted ionic clusters.

DATA AVAILABILITY STATEMENT

The data that support the findings of this study are available from the corresponding author upon reasonable request.

REFERENCES

[1] E. Dale, B. Jorns, and A. Gallimore, "Future directions for electric propulsion research," Aerospace **7**, 120 (2020).
[2] M. Gamero-Castaño and V. Hruby, "Electrospray as a source of nanoparticles for efficient colloid thrusters," Journal of Propulsion and Power **17**, 977–987 (2001).
[3] A. Quraishi, S. Dworski, E. Batchelor, A. Gonzalez Machado, C. Ryan, A. Ferreri, G. Vincent, A. Croos, A. Garbayo, M. Vozarova, *et al.*, "Development of a 50 w porous emitter electrospray thruster towards flight," in *74th International Astronautical Congress* (2023).
[4] M. R. Natisin, H. L. Zamora, Z. A. Holley, N. Ivan Arnold, W. A. McGehee, M. R. Holmes, and D. Eckhardt, "Efficiency mechanisms in porous-media electrospray thrusters," Journal of Propulsion and Power **37**, 650–659 (2021).
[5] D. Krejci, F. Mier-Hicks, R. Thomas, T. Haag, and P. Lozano, "Emission characteristics of passively fed electrospray microthrusters with propellant reservoirs," Journal of Spacecraft and Rockets **54**, 447–458 (2017).
[6] D. G. Courtney, N. Alvarez, and N. R. Demmons, "Electrospray thrusters for small spacecraft control: Pulsed and steady state operation," in *2018 Joint Propulsion Conference* (2018) p. 4654.
[7] C. Ma, *Design and characterisation of electrospray thrusters with high emission density*, Ph.D. thesis, University of Southampton, Department of Aeronautical and Astronautical … (2020).
[8] M. N. Sweeting, "Modern small satellites-changing the economics of space," Proceedings of the IEEE **106**, 343–361 (2018).
[9] A. R. Katritzky, R. Jain, A. Lomaka, R. Petrukhin, M. Karelson, A. E. Visser, and R. D. Rogers, "Correlation of the melting points of potential ionic liquids (imidazolium bromides and benzimidazolium bromides) using the codessa program," Journal of chemical information and computer sciences **42**, 225–231 (2002).
[10] A. Quraishi, S. Dworski, C. Ma, C. Ryan, A. Ferreri, G. Vincent, H. Larsen, E. R. Azevedo, E. Dingle, A. Garbayo, *et al.*, "Development of porous emitter electrospray thruster using advanced manufacturing processes," in *37th International Electric Propulsion Conference* (2022).
[11] J. F. De La Mora and I. G. Loscertales, "The current emitted by highly conducting taylor cones," Journal of Fluid Mechanics **260**, 155–184 (1994).
[12] R. J. Pfeifer and C. D. Hendricks, "Parametric studies of electrohydrodynamic spraying." AIAA Journal **6**, 496–502 (1968), https://doi.org/10.2514/3.4525.
[13] D. Garoz, C. Bueno, C. Larriba, S. Castro, I. Romero-Sanz, J. Fernandez de La Mora, Y. Yoshida, and G. Saito, "Taylor cones of ionic liquids from capillary tubes as sources of pure ions: The role of surface tension and electrical conductivity," Journal of Applied Physics **102** (2007).
[14] S. Castro, C. Larriba, J. Fernandez de La Mora, P. Lozano, S. Sümer, Y. Yoshida, and G. Saito, "Effect of liquid properties on electrosprays from externally wetted ionic liquid ion sources," Journal of Applied Physics **102** (2007).
[15] R. Legge and P. Lozano, "Performance of heavy ionic liquids with porous metal electrospray emitters," in *44th AIAA/ASME/SAE/ASEE Joint Propulsion Conference & Exhibit* (2008) p. 5002.
[16] J. Iribarne and B. Thomson, "On the evaporation of small ions from charged droplets," The Journal of chemical physics **64**, 2287–2294 (1976).
[17] C. S. Coffman, M. Martínez-Sánchez, and P. C. Lozano, "Electrohydrodynamics of an ionic liquid meniscus during evaporation of ions in a regime of high electric field," Physical Review E **99**, 063108 (2019).
[18] P. C. Lozano-Tovar, *Studies on the ion-droplet mixed regime in colloid thrusters*, Ph.D. thesis, Massachusetts Institute of Technology (2003).
[19] I. G. Loscertales and J. Fernández De La Mora, "Experiments on the kinetics of field evaporation of small ions from droplets," The Journal of chemical physics **103**, 5041–5060 (1995).
[20] C. E. Miller, *Characterization of ion cluster fragmentation in ionic liquid ion sources*, Ph.D. thesis, Massachusetts Institute of Technology (2019).
[21] M. Geppert-Rybczynska, J. K. Lehmann, T. Peppel, M. Kockerling, and A. Heintz, "Studies of physicochemical and thermodynamic properties of the paramagnetic 1-alkyl-3-methylimidazolium ionic liquids (emim) 2 [co (ncs) 4] and (bmim) 2 [co (ncs) 4]," Journal of Chemical & Engineering Data **55**, 5534–5538 (2010).

[22]M. Chakraborty, S. Barik, A. Mahapatra, and M. Sarkar, "Effect of lithium-ion on the structural organization of monocationic and dicationic ionic liquids," The Journal of Physical Chemistry B **125**, 13015–13026 (2021).
[23]X. Gallud and P. C. Lozano, "The limited effect of electric conductivity on the ion current evaporated from electrospray sources," arXiv preprint arXiv:2305.14714 (2023).
[24]C. Larriba, S. Castro, J. Fernandez De La Mora, and P. Lozano, "Monoenergetic source of kilodalton ions from taylor cones of ionic liquids," Journal of applied physics **101** (2007).
[25]P. W. Atkins, J. De Paula, and J. Keeler, *Atkins' physical chemistry* (Oxford university press, 2006) p. 102.
[26]C. Ma and C. Ryan, "Plume particle energy analysis of an ionic liquid electrospray ion source with high emission density," Journal of Applied Physics **129** (2021).
[27]N. Turan, C. Ma, and C. N. Ryan, "Optical emission characterization of a single emitter electrospray thruster interacting with surfaces," in *AIAA SCITECH 2023 Forum* (2023) p. 1409.
[28]S. Castro and J. Fernández De La Mora, "Effect of tip curvature on ionic emissions from taylor cones of ionic liquids from externally wetted tungsten tips," Journal of applied physics **105** (2009).
[29]P. C. Lozano, "Energy properties of an emi-im ionic liquid ion source," Journal of Physics D: Applied Physics **39**, 126 (2005).
[30]I. Romero-Sanz, R. Bocanegra, J. Fernandez De La Mora, and M. Gamero-Castaño, "Source of heavy molecular ions based on taylor cones of ionic liquids operating in the pure ion evaporation regime," Journal of Applied Physics **94**, 3599–3605 (2003).
[31]D. G. Courtney and H. Shea, "Influences of porous reservoir laplace pressure on emissions from passively fed ionic liquid electrospray sources," Applied Physics Letters **107** (2015).
[32]M. Natisin, H. Zamora, W. McGehee, N. Arnold, Z. Holley, M. Holmes, and D. Eckhardt, "Fabrication and characterization of a fully conventionally machined, high-performance porous-media electrospray thruster," Journal of Micromechanics and Microengineering **30**, 115021 (2020).
[33]We thank Professor Patricia Hunt from the Victoria University of Wellington for giving us insight into the chemical reason why the doubly charged ionic liquids may tend to emit very few monomers.
[34]M. Gamero-Castano and J. F. De La Mora, "Mechanisms of electrospray ionization of singly and multiply charged salt clusters," Analytica Chimica Acta **406**, 67–91 (2000).